Polarization and Differential Cross Section for Elastic Scattering of 40-MeV Protons. II*

M. P. FRICKE,† E. E. GROSS, B. J. MORTON,‡ AND A. ZUCKER
Oak Ridge National Laboratory, Oak Ridge, Tennessee
(Received 28 November 1966)

Polarization and differential-cross-section data are presented for the elastic scattering of 40-MeV protons from eleven targets: ^{12}C, ^{28}Si, ^{40}Ca, ^{54}Fe, ^{58}Ni, ^{59}Co, ^{60}Ni, ^{68}Zn, ^{90}Zr, ^{120}Sn, and ^{208}Pb. These data were analyzed with a 10-parameter optical model from which "average parameters" were obtained. The average parameters provide a good fit to our data and lead to a value of about 26 MeV for the depth of the symmetry part of the real central potential. Satisfactory fits to existing 30-MeV data are also realized with these average parameters which, together with the fits to the 40-MeV data, result in an energy dependence of the real central potential of about -0.22 MeV per MeV increase in proton beam energy. Behavior of the $l=0$ optical-model reflection coefficients is studied as a function of A and appears to be consistent with a mean free path for a reaction in nuclear matter of about 7 F.

I. INTRODUCTION

POLARIZED and unpolarized 40-MeV proton beams from the Oak Ridge Isochronous Cyclotron (ORIC) were used to continue a systematic study of the polarization and differential cross section for elastic scattering from a variety of nuclei. In a previous paper,[1] hereinafter referred to as I, we reported on experiments with five targets; in this paper we report on six additional targets: ^{28}Si, ^{54}Fe, ^{59}Co, ^{60}Ni, ^{68}Zn, and ^{120}Sn. The essential improvement in our apparatus which has enabled us to investigate these new targets was the addition of magnetic-energy analysis of the polarized beam. We could now use targets with fairly low-lying excited states and still avoid the peril of confusing elastic with inelastic scattering events.

Since the publication of I, we have made a more accurate determination of the absolute polarization of the polarized proton beam. A few other changes were made in the experimental procedure, but by and large this paper is essentially a continuation of I. Here we treat all eleven targets and collect the results of measurements described in both papers. This is necessary because of our new determination of the value of the beam polarization. Our results are compared with optical-model calculations for all eleven targets. These represent a better sample from which to draw conclusions regarding the systematics of the optical model, for example, the nuclear-symmetry term in the real potential. Entirely new optical-model calculations were performed on the five targets reported in I.

II. THE EXPERIMENT

The polarized beam was produced by scattering 50-MeV protons from a 10-MeV-thick calcium target. It was then transported through a 7-ft shield wall to the scattering chamber in which the target is surrounded by 32 NaI(Tl) detectors arranged symmetrically on the left and right side of the beam. The angular acceptance of the counters was $\pm 1.2°$ for the polarization measurements and $\pm 0.4°$ for the differential-cross-section measurements. The solid angles subtended by the counters are known to $\pm 1\%$, and the beam direction and detector position were determined to $\pm 0.1°$. A 20 000-channel analyzer was used as fifty 400-channel analyzers for this experiment. We will not describe the experiment in detail, since this has been done in I, or in another paper devoted entirely to the polarized-proton facility.[2]

A. Magnetic Analysis of the Polarized Beam

A serious limitation in the measurement of the polarization for elastic scattering at 40 MeV is imposed by the requirement that the elastic events be clearly resolved from inelastically scattered protons. In our previous arrangement the polarized proton beam had an energy spread of 600 keV FWHM (full width at half-maximum) when using a Ca polarizer, and 1.4 MeV from the α-p source. To this must be added the resolution of the 32 NaI(Tl) detectors which varied from 350 keV to 500 keV from one detector to another.

To achieve an adjustable energy spread in the polarized proton beam, and to eliminate protons inelastically scattered from the calcium target, we added an analyzing magnet to the polarized-proton transport system. The entire setup is shown in Fig. 1, and works as follows. An unpolarized beam of 50-MeV protons is focused on a 10-MeV-thick Ca target (polarizer) to a spot about 2 mm high and 8 mm wide. Protons scattered at 25.5° are made parallel by the first quadrupole doublet and are brought to a horizontal focus by the second quadrupole doublet on the entrance slit of the analyzing magnet. The analyzing magnet and the

* Research sponsored by the U. S. Atomic Energy Commission under contract with the Union Carbide Corporation.
† Oak Ridge Graduate Fellow from the University of Minnesota under appointment from Oak Ridge Associated Universities.
‡ Oak Ridge Graduate Fellow from the University of Tennessee under appointment from Oak Ridge Associated Universities.
[1] L. N. Blumberg, E. E. Gross, A. van der Woude, A. Zucker, and R. H. Bassel, Phys. Rev. **147**, 812 (1966).

[2] L. N. Blumberg, E. E. Gross, A. van der Woude, and A. Zucker, Nucl. Instr. Methods **39**, 125 (1966).

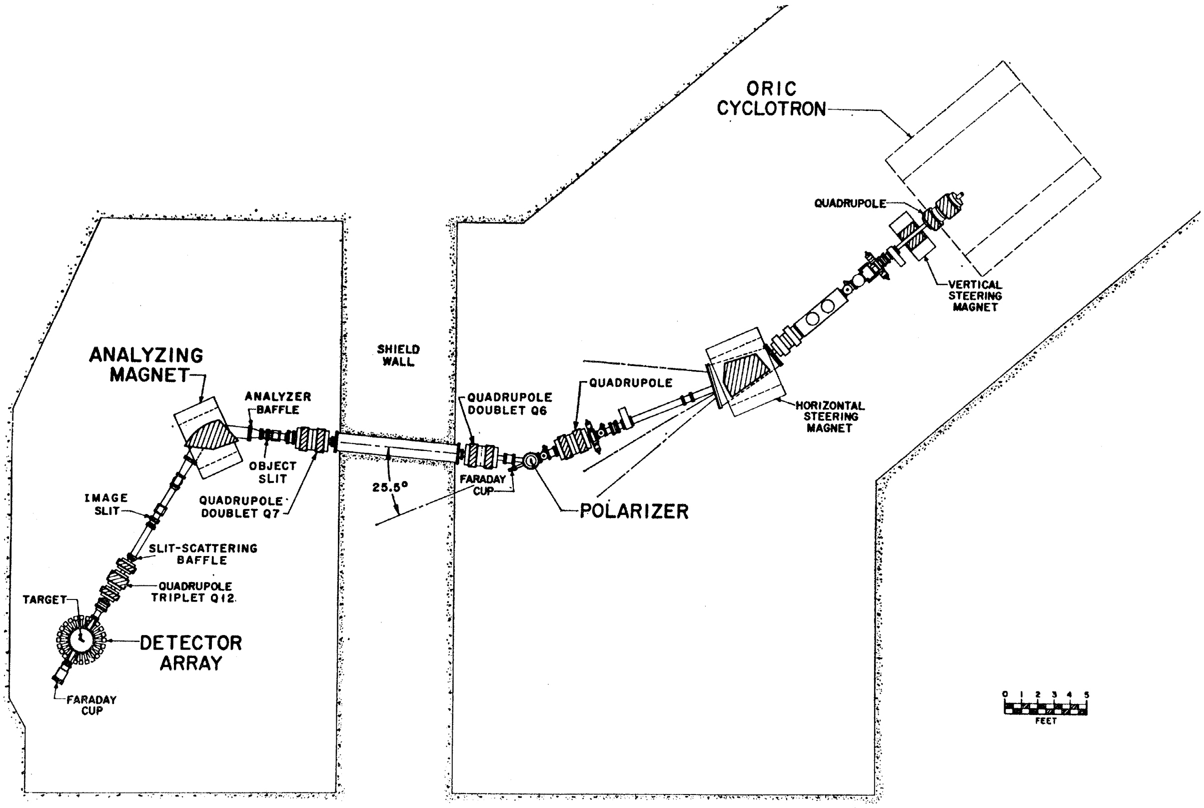

FIG. 1. Arrangement of beam optics to obtain magnetic analysis of the polarized beam.

second quadrupole doublet together produce a beam which is focused vertically and horizontally on the exit slit. This slit serves as the object of a quadrupole triplet which focuses the beam to a spot 4 mm wide by 11 mm high at the center of the scattering chamber. The angular divergence of the beam is $\pm 2°$ in the horizontal (scattering) plane. The entrance and exit slits of the magnet can be reduced to obtain the desired resolution, at the expense of beam intensity. For the experiments reported here we used beams with an energy spread in the range 300 to 500 keV FWHM, and the over-all resolution was 500 to 800 keV. With 10 μA of protons incident on a 10-MeV-thick Ca polarizer, and with 500-keV beam spread, we obtained about 10^8 protons/sec on the target. In addition to providing energy analysis, the new beam transport system results in an exceptionally low background at the detector array. In our previous arrangement described in I, neutrons from the polarizer presented serious difficulties in the detectors located at angles greater than 120°. The addition of the analyzing magnet seems to have overcome this problem.

The energy of the magnetically analyzed beam was measured by NaI pulse-height variation for different absorbers placed before the crystal detector. This same method had been used to set the beam energy in our previous work, both with the polarized and unpolarized beams. In many runs the energy was also measured by residual range in emulsion. A comparison of both measurements revealed a constant difference of about 1 MeV between the two methods. A recent comparison with a magnetic rigidity determination, good to $\frac{1}{2}\%$ in energy, confirmed the correctness of the emulsion method. Although the source of error in the NaI energy measurement is still not understood, the method has proved to be consistent; the speed and ease of this method were essential in setting the cyclotron energy for each of the many runs that comprise this work. As a result of these energy measurements, we can state that all the data presented here were obtained with proton energies of 40.0 ± 0.4 MeV.

B. Measurement of the Beam Polarization

In our previous work[1] we were able to measure the absolute value of the beam polarization only to $\pm 8.5\%$. The reason for such a large uncertainty is the difficulty of a double-scattering measurement from Ca at 25.5°, for which very careful alignment is required. Even with alignments as good as $\pm 0.05°$, we found it impossible to reproduce to any greater precision the absolute value of the polarization.

In the meantime it came to our attention that a very good measurement had been made of the polarizing

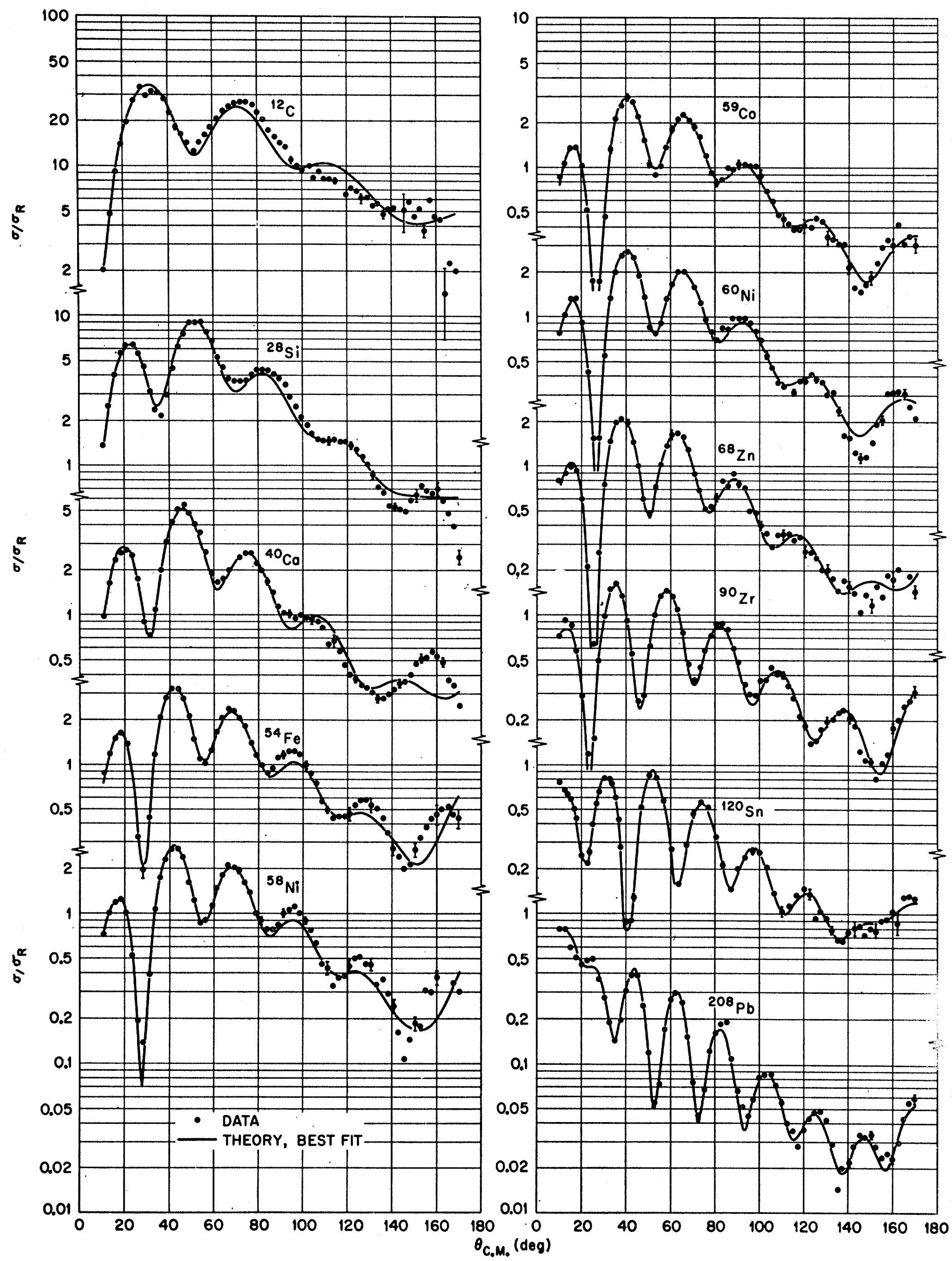

FIG. 2. Ratio-to-Rutherford differential cross sections for 40-MeV elastic proton scattering from various nuclei. Data for ^{12}C, ^{40}Ca, ^{58}Ni, ^{90}Zr, and ^{208}Pb are reproduced from Ref. 1. Typical statistical error bars are shown. The solid curves represent the best simultaneous fits to the cross-section and polarization data. Corresponding optical-model parameters are shown in Table II.

power of carbon,[3] P_C, at 27.5 MeV and at 65° lab. At this angle the differential cross section as well as the polarization for carbon are both slowly varying functions of angle, and the measurement is not fraught with the difficulties which beset the calcium double-scattering measurement. Our new beam-polarization measurement is then based on the 27.5-MeV result which gives $P_C=0.558\pm0.010$ at 65° lab. To make use of this result we placed an absorber in the 40-MeV beam to

[3] R. M. Craig, J. C. Dore, G. W. Greenlees, J. S. Lilley, J. Lowe, and P. C. Rowe, Nucl. Instr. Methods 30, 268 (1964); J. C. Dore (private communication).

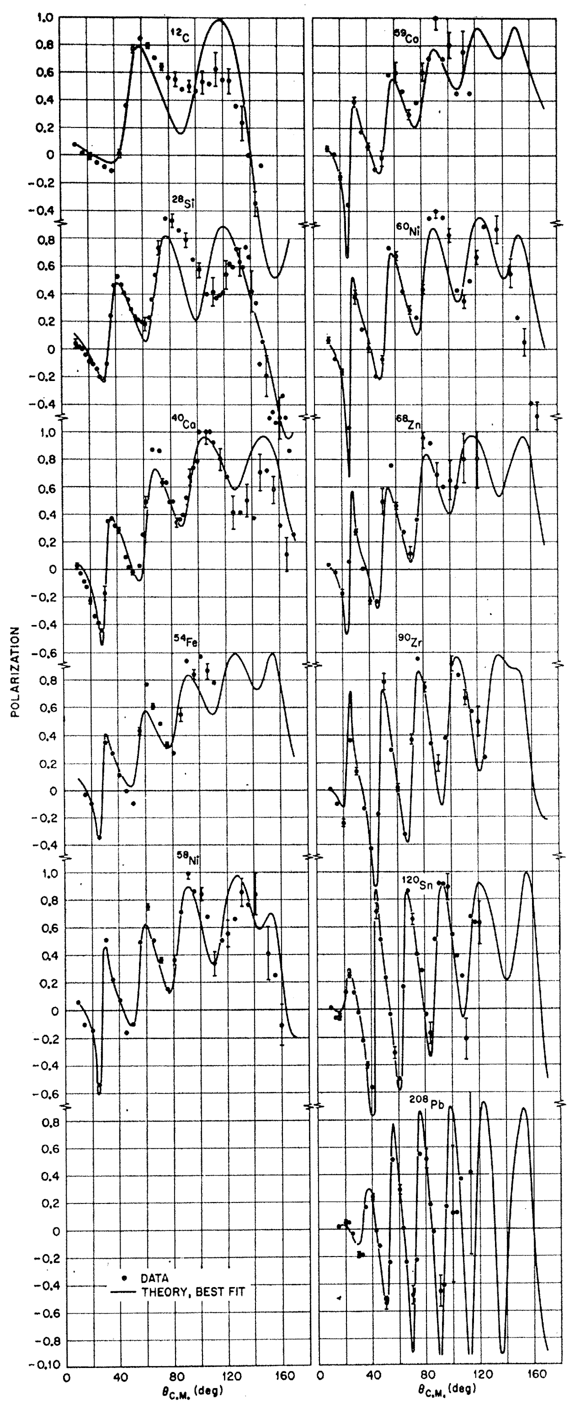

FIG. 3. Polarization versus center-of-mass angle for 40-MeV elastic proton scattering from various nuclei. Data for ^{12}C, ^{40}Ca, ^{58}Ni, ^{90}Zr, and ^{208}Pb are those from Ref. 1 corrected by the new measurement of beam polarization. Typical statistical error bars are shown. The solid curves represent the simultaneous fits to the cross-section and polarization data using the parameters of Table II.

reduce its energy to 27.5 MeV while affecting the proton polarization a negligible amount.[4,5] The asymmetry ϵ was measured at 65° lab, and the polarization P_B of the 40-MeV beam is ascertained from the relation $\epsilon = P_B P_C$. Our result is that the polarization of the 40-MeV beam is $(27.4 \pm 0.5)\%$, including the uncertainty in P_C. This value of P_B was used to revise the polarization measurements on the five targets reported in I, and it improves significantly the accuracy of our results.

Two problems that continually plague double-scattering measurements are the precise determination of the beam-spot position on the second target and the beam direction. We have recently built a split ion chamber[6] which can be placed accurately at the target position in the scattering chamber. With this instrument we are able to place the beam in the geometric center of the counter array to within ± 0.1 mm. This is a considerable improvement over our previous photographic method which was good to ± 0.4 mm. The beam direction is still ascertained by measuring scattering from Pb at 10° and is known to $\pm 0.1°$.

C. Targets

The targets used in this experiment are given in Table I. Again the measurement of the target thickness introduced the most serious errors into the absolute normalization of the differential cross section. Thick-thin target ratios were obtained as described in I; the differential cross sections were normalized in the same way.

The reader is also referred to I for a description of the scattering chambers, detectors, electronics, running and alignment procedures, and other experimental details.

III. RESULTS

In this paper we present results in graphical form for the differential cross section, Fig. 2, and polarization, Fig. 3, for all eleven elements measured so far. The differential cross sections for five of them, ^{12}C, ^{40}Ca,

TABLE I. Targets.

Isotope	Isotopic purity (%)	Thickness (mg/cm^2)
^{12}C	98.9	48.4
^{28}Si	92.2	32.1
^{40}Ca	97.0	25.4
^{54}Fe	97.4	18.0
^{58}Ni	99.95	29.95
^{59}Co	100	19.68
^{60}Ni	99.1	19.25
^{68}Zn	98.5	23.61
^{90}Zr	97.8	19.46
^{120}Sn	98.4	23.18
^{208}Pb	98.0	26.48

[4] L. Wolfenstein, Phys. Rev. **75**, 1664 (1949).

[5] E. Heiberg, E. Kruse, J. Marshall, L. Marshall, and F. Solmitz, Phys. Rev. **97**, 250 (1955).

[6] We are indebted to R. C. Hanna for supplying the design of the split ion chamber.

TABLE II. Optical-model parameters from least-squares search of 40-MeV elastic-cross-section and polarization data which yielded minimum χ^2.

	^{12}C	^{28}Si	^{40}Ca	^{54}Fe	^{58}Ni	^{59}Co	^{60}Ni	^{68}Zn	^{90}Zr	^{120}Sn	^{208}Pb
V_0 (MeV)	38.38	41.11	41.55	41.43	49.49	45.65	48.28	47.43	45.95	48.36	54.62
W_0 (MeV)	2.94	3.19	1.56	6.40	6.50	6.06	5.41	6.94	3.21	4.62	5.31
r_0 (F)	1.182	1.178	1.203	1.208	1.109	1.151	1.120	1.155	1.186	1.168	1.125
a (F)	0.624	0.709	0.674	0.761	0.782	0.759	0.769	0.751	0.674	0.746	0.873
V_s (MeV)	6.18	6.47	6.22	5.30	5.53	6.01	7.03	5.72	6.92	6.11	5.84
r_0' (F)	1.910	1.560	1.255	1.279	1.477	1.397	1.470	1.318	1.300	1.322	1.386
a' (F)	0.016	0.486	0.704	0.609	0.495	0.718	0.597	0.689	0.655	0.728	0.624
W_D (MeV)	5.12	1.98	4.92	2.47	0.52	1.12	1.58	0.28	5.25	4.39	5.60
a_s (F)	0.517	0.741	0.778	0.679	0.641	0.846	0.856	0.720	0.861	0.800	0.794
r_s (F)	1.109	1.089	1.028	1.188	1.071	1.010	0.979	1.040	1.002	1.057	1.026
χ_σ^2/N_σ	13.7	23.7	10.0	3.8	5.4	1.9	6.0	9.1	16.3	2.7	23.4
χ_P^2/N_P	36.5	11.9	8.5	23.3	25.0	5.3	17.8	5.3	24.3	5.5	9.0
$\sigma_{R\text{ca'o}}$ (mb)	316	638	858	990	1023	1111	1126	1262	1375	1704	2217

^{58}Ni, ^{90}Zr, and ^{208}Pb, are taken directly from I, but the polarizations have been adjusted in line with our new measurement of the beam polarization. We do not present our data in tabular form. Such tables exist and, as long as the supply lasts, they will be sent upon request. The tabular material is on file with the American Documentation Institute[7] and copies may be procured from it.

The polarization $P(\theta)$ is obtained from the incident-beam polarization P_B and the measured left-right asymmetry, $P(\theta)=\epsilon(\theta)/P_B$. We follow the Basel convention; the asymmetry $\epsilon(\theta)$ is

$$\epsilon(\theta)=\frac{L(\theta)-R(\theta)}{L(\theta)+R(\theta)},$$

where L is the number of counts on the left, and R is the number of counts on the right.

The error bars in Figs. 2 and 3 are relative probable errors which include statistical errors and the uncertainty in background subtraction. The fractional error in the asymmetry $\Delta\epsilon/\epsilon$ is calculated from ΔL and ΔR, the errors in L and R, from the relation

$$\frac{\Delta\epsilon(\theta)}{\epsilon(\theta)}=2\left[\left(\frac{L\Delta R}{L^2-R^2}\right)^2+\left(\frac{R\Delta L}{L^2-R^2}\right)^2\right]^{1/2}.$$

Relative errors in the differential-cross-section measurement are chiefly statistical. In addition there is an absolute error of $\pm5\%$ due to the uncertainty in determining the target thickness. Corrections were made for the loss of counts from the elastic peak caused by reactions in the crystal.[8] Multiple-scattering corrections were unnecessary.

IV. OPTICAL-MODEL ANALYSIS

An optical-model analysis was performed with the following form of the local potential:

$$V(r)=V_c(r)-V_0\left(\frac{1}{e^x+1}\right)-i\left(W_0-4W_D\frac{d}{dx'}\right)\frac{1}{e^{x'}+1}$$
$$+\left(\frac{h}{m_\pi c}\right)^2 V_s\frac{1}{r}\frac{d}{dr}\left(\frac{1}{e^{x_s}+1}\right)\boldsymbol{\sigma}\cdot\mathbf{l}.$$

In this expression $V_c(r)$ is the Coulomb potential for a uniformly charged sphere of radius $1.25A^{1/3}$ F, V_0 is the real potential, W_0 and W_D are the volume and surface parts, respectively, of the imaginary potential, and V_s is the real part of the spin-orbit potential. The imaginary part of the spin-orbit potential was always set to zero, since its value turns out to be very small in all cases we have encountered. The remaining factors in the optical potential contain the Woods-Saxon radius and diffusivity parameters: $x=(r-R)/a$, $x'=(r-R')/a'$, $x_s=(r-R_s)/a_s$, $R=r_0A^{1/3}$, $R'=r_0'A^{1/3}$, $R_s=r_sA^{1/3}$; m_π is the pion mass.

First, each target was analyzed independently with the ten-parameter potential, and a best simultaneous fit was obtained to the polarization and differential-cross-section data. In Table II we list the values of the best-fit parameters, total reaction cross sections, and the value of X^2 for the cross section and polarization separately. Here

$$\chi_\sigma^2=\sum_{i=1}^{N_\sigma}\frac{[\sigma_{\text{theor}}(\theta_i)-\sigma_{\text{expt}}(\theta_i)]^2}{\Delta\sigma(\theta_i)^2}$$

and

$$\chi_P^2=\sum_{i=1}^{N_P}\frac{[P_{\text{theor}}(\theta_i)-P_{\text{expt}}(\theta_i)]^2}{\Delta P(\theta_i)^2}.$$

[7] Copies of the tables may be obtained at $2.00 per microfilm copy and $3.75 per photo-copy by writing to the American Documentation Institute, Auxiliary Publication Project, Library of Congress, Washington, D. C. 20036.

[8] D. F. Measday, Nucl. Instr. Methods 34, 353 (1956).

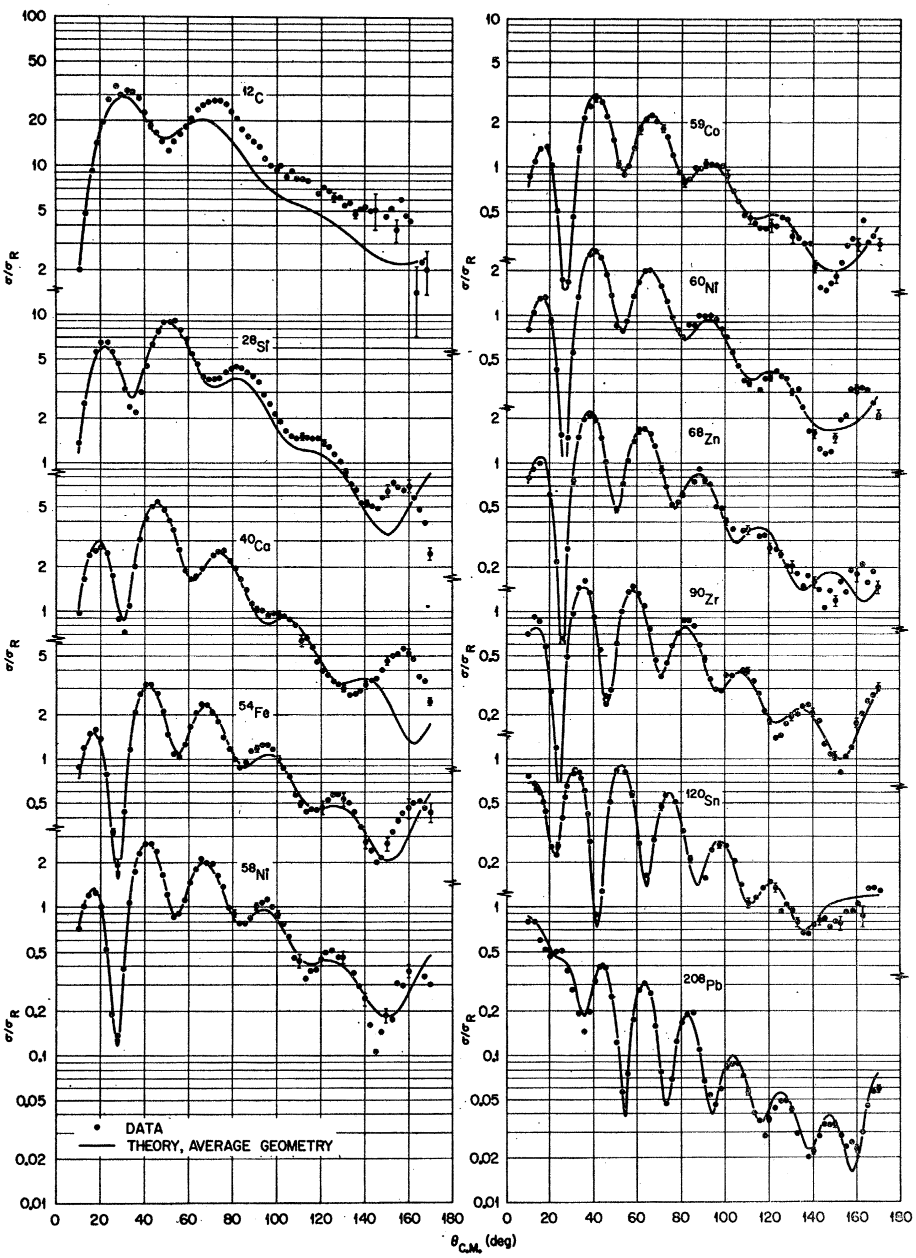

FIG. 4. Average-parameter fits to the 40-MeV elastic proton scattering data. The solid curves result from a search on V_0, W_0, and W_D for a simultaneous fit to cross-section and polarization data using the average parameters given in the text. The resulting values of V_0, W_0, and W_D are shown in Table III.

The calculation was done with the program HUNTER[9] to obtain a simultaneous minimization of both χ_σ^2 and χ_P^2. As is well known, this procedure is fraught with pitfalls, since the search program may exert itself to fit the points with the smallest experimental errors at the expense of a general fit to the gross features of the

TABLE III. Central well strengths, reaction cross sections, and χ^2 values resulting from average-geometry fits to 40-MeV data.

	^{12}C	^{28}Si	^{40}Ca	^{54}Fe	^{58}Ni	^{59}Co	^{60}Ni	^{68}Zn	^{90}Zr	^{120}Sn	^{208}Pb
V_0 (MeV)	38.29	42.38	43.22	45.79	45.05	45.71	45.74	46.60	47.76	48.77	52.76
W_0 (MeV)	8.72	4.00	1.21	6.89	6.63	5.68	5.47	6.70	4.69	4.72	6.12
W_D (MeV)	1.18	1.96	4.52	1.14	1.22	2.08	2.5	2.46	3.46	4.62	4.31
χ_σ^2/N_σ	57.1	43.8	20.2	6.6	6.4	3.1	7.7	10.7	35.1	3.4	56.5
χ_P^2/N_P	244.2	22.3	18.3	66.1	37.4	5.7	18.9	7.0	8.2	9.3	9.4
$\sigma_{R\text{calc}}$ (mb)	316	630	841	1015	1046	1088	1118	1250	1410	1691	2116

[9] R. M. Drisko (private communication).

data. In a few cases we adjusted the weights of some points with small experimental errors to decrease their influence on the fitting procedure. In addition, we examined the agreement between the data and the calculation in a subjective fashion, and discarded those fits which seemed to satisfy the minimum χ^2 criteria at the expense of an over-all shape agreement. With the exception of the separate polarization study described in the next section, the parameters obtained by including the "esthetic" criterion differ only slightly from those which rely only on χ^2. The conclusions we reach in the ensuing discussion would not be altered significantly if we had not included this "esthetic" criterion. The results of the calculations and the data are shown in Figs. 2 and 3.

In our calculations, the starting values for the geometrical parameters for the HUNTER searches were the average values found in I. We cannot claim to have examined all possibilities in the ten-parameter space, but, as can be seen from Figs. 2 and 3, we have achieved reasonably good fits for all elements, except possibly ^{12}C.

Once the data for each target had been analyzed in this fashion, the geometrical parameters for the best fits shown in Table II, leaving out ^{12}C, were averaged and fixed at the following values:

$$r_0=1.16\text{ F},\quad r_0'=1.37\text{ F},\quad r_s=1.064\text{ F},$$

$$a=0.75\text{ F},\quad a'=0.63\text{ F},\quad a_s=0.738\text{ F}.$$

In addition, V_s was fixed at its average of 6.04 MeV, since it does not appear to vary systematically from one nucleus to another. We were thus left with three adjustable parameters: V_0, W_0, and W_D. All our data, polarizations and differential cross sections for eleven targets, were then fitted with the fixed-geometry parameters listed above, and the values of V_0, W_0, and W_D determined in this way are given in Table III. Again, we used a combination of χ^2 minimization and esthetic criteria to ascertain the best fit. In Figs. 4 and 5, we show the agreement between fixed-geometry calculations and the experimental results.

It can be seen that, except for ^{12}C, the quality of the fits with fixed geometry appears to be as good as that of the best fits to each individual target. The fixed-geometry fits, however, have values of χ^2 which are 1.5 to 2.5 times greater than those for the ten-parameter fits. Within this limitation, we conclude that the above average parameters provide a reasonable optical-model description of the present data for elastic scattering and polarization of protons at 40 MeV.

It is of interest to see how well the above average parameters can account for similar data for a proton energy near 30 MeV.[10,11] Resulting fits for a number of isotopes are shown in Figs. 6 and 7 for the parameter values given in Table IV. We neglect the fact that the polarization data were obtained at 29 MeV, a complication which was examined in detail by Satchler.[12] Qualitatively the agreement looks good but has χ^2 values which average about 3.5 times greater than those

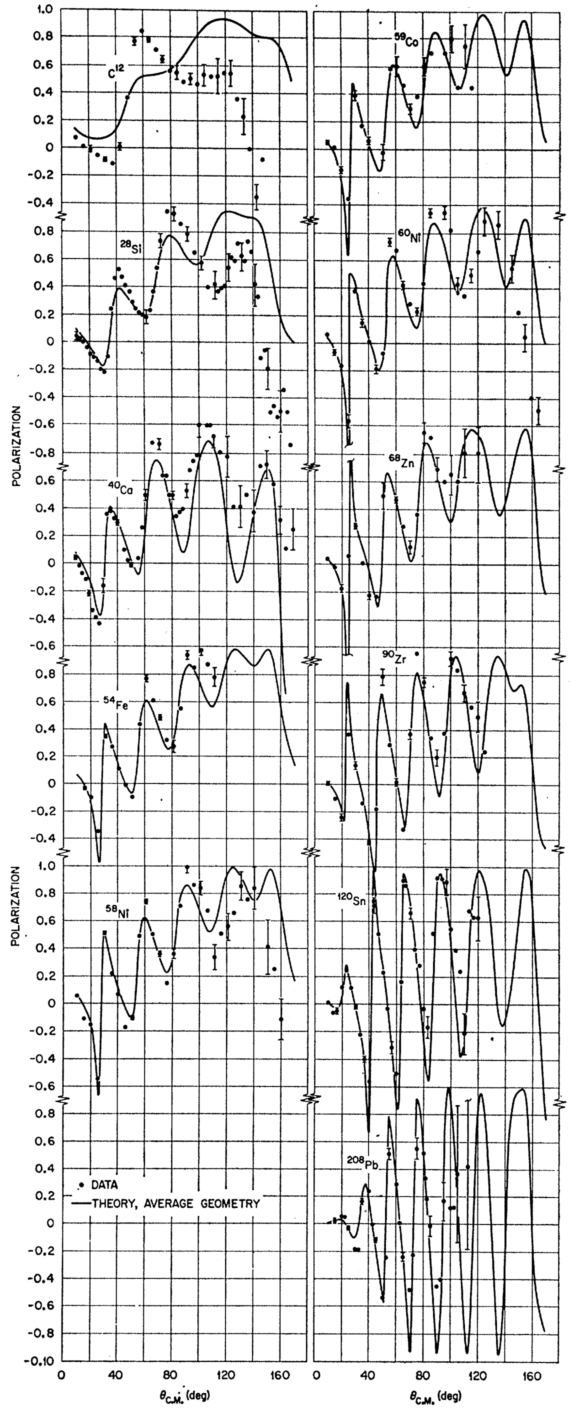

FIG. 5. Average-parameter fits to the 40-MeV proton polarization data. The solid curves correspond to the cross-section fits shown in Fig. 4.

[10] B. W. Ridley and J. F. Turner, Nucl. Phys. 58, 497 (1964).
[11] R. M. Craig, J. C. Dore, G. W. Greenlees, J. S. Lilley, and J. Lowe, Nucl. Phys. 58, 515 (1964).
[12] G. R. Satchler, Nucl. Phys. A92, 273 (1967).

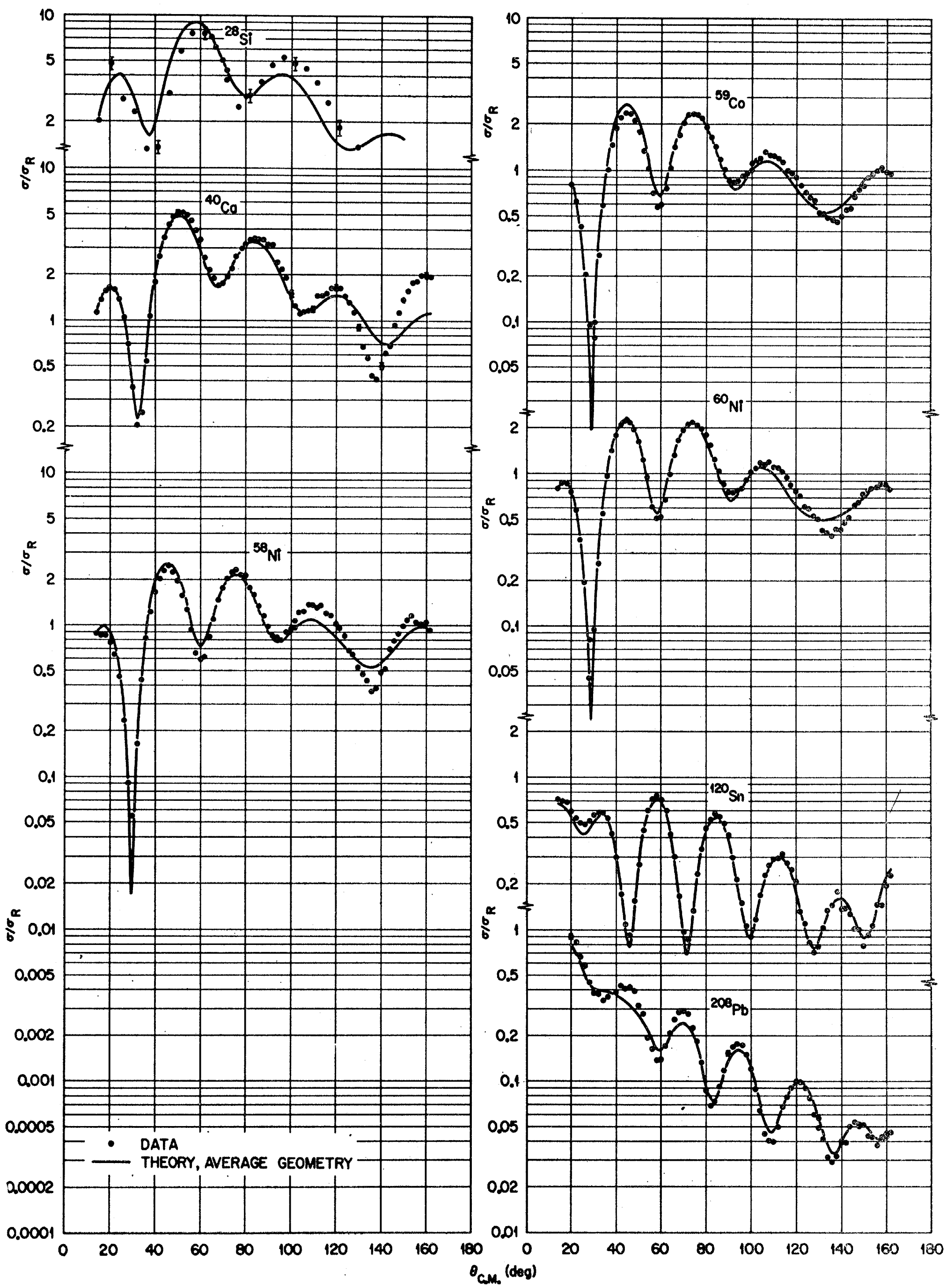

FIG. 6. Average-parameter fits to the 30-MeV elastic proton scattering data (Ref. 10). The solid curves result from the average parameters given in the text and the central potential strengths shown in Table IV.

obtained[12] with ten-parameter searches. Also, the agreement appears to be comparable to a recent analysis[13] using slightly different parameters and considerably better than an earlier analysis[14] using the geometry parameters suggested by Perey[15] for lower-energy scattering. Thus, the average optical-model parameters found here afford a reasonable description of elastic proton scattering and polarization in the range 30–40 MeV and should provide a useful starting point for more elaborate searches. At 28.5 MeV, there are reaction-cross-section measurements[16] which can be

[13] G. W. Greenlees and G. J. Pyle, Phys. Rev. **149**, 836 (1966).
[14] R. C. Barrett, A. D. Hill, and P. E. Hodgson, Nucl. Phys. **62**, 133 (1965).
[15] F. G. Perey, Phys. Rev. **131**, 745 (1963).
[16] J. F. Turner, B. W. Ridley, P. E. Cavanagh, G. A. Gord, and A. G. Hardacre, Nucl. Phys. **58**, 509 (1964).

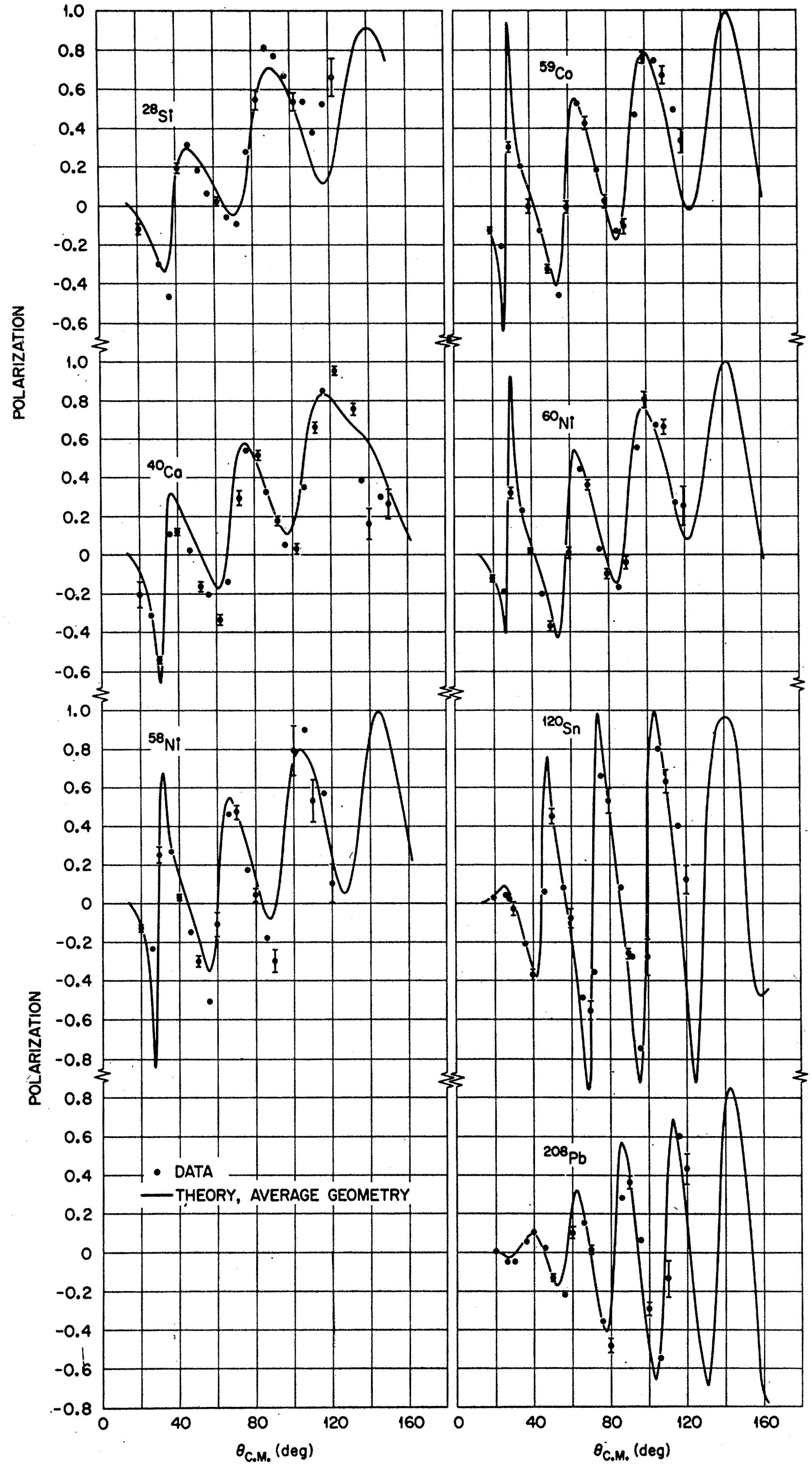

FIG. 7. Average-parameter fits to the 30-MeV proton polarization data (Ref. 11). The solid curves correspond to the cross-section fits shown in Fig. 6.

compared with predictions of the optical model. It can be seen in Table IV that the average geometry potential yields reaction cross sections which are in very good agreement with the experimental results.

V. DISCUSSION

An optical-model analysis of the sort described above yields some qualitative results which we shall summarize in this section.

TABLE IV. Central well strengths, reaction cross sections, and χ^2 values resulting from average-geometry fits to 30-MeV data.

	^{28}Si	^{40}Ca	^{56}Fe	^{58}Ni	^{59}Co	^{60}Ni	^{120}Sn	^{208}Pb
V_0 (MeV)	44.30	47.38	49.10	46.03	47.13	48.22	51.08	56.12
W_0 (MeV)	0.96	2.24	5.70	2.65	1.78	3.21	4.18	6.51
W_D (MeV)	3.97	4.22	1.42	3.75	4.97	4.11	5.26	4.04
χ_σ^2/N_σ	6.6	43.4	3.0	24.5	22.9	17.5	8.8	13.6
χ_P^2/N_P	13.7	29.3	⋯	12.3	47.2	40.9	31.2	17.7
$\sigma_{R\mathrm{calc}}$ (mb)	717	940	1147	1096	1150	1180	1668	1920
$\sigma_{R\mathrm{expt}}{}^{(16)}$ (mb)	⋯	913±38	1140±43	1038±32	1169±39	1053±51	1638±68	1865±98

First, one can draw certain conclusions about the trends of the geometrical parameters. We find consistently that the imaginary radius r_0' is larger than the real radius r_0 and that r_s, the spin-orbit radius, is smaller than either r_0 or r_0'. These conclusions are not new, we have made them before,[1,17] and others have also.[12,13,18] We also repeat our previous conclusions (see I) that volume as well as surface absorption is needed for good fits for targets heavier than calcium.

While it is generally agreed that both cross-section and polarization data are desirable, their relative influence in establishing the values of specific parameters is not yet clear. For three targets, ^{28}Si, ^{58}Ni, and ^{60}Ni, some additional calculations were made to improve the fits to the polarizations, principally at back angles, at the expense of the fits to the cross sections. This was done with simultaneous σ-P searches by assigning large weights (small errors) to the large-angle polarization data, as opposed to the experimental uncertainties used to weight χ_P^2 in the analysis given above. For each of these targets, a potential was obtained which had a decidedly smaller value of r_0, and a larger value of a, than the best-fit values (Table II), while the other parameters were generally similar to the best values. By emphasizing large-angle polarization data we obtain a potential for ^{60}Ni with $r_0=1.08$ F and $a=0.82$ F, as opposed to the best-fit values of $r_0=1.12$ F and $a=0.77$ F, and the average-geometry results of $r_0=1.16$ F and $a=0.75$ F. It is therefore interesting to contemplate whether accurate polarization data beyond 140° would lead to average-geometry parameters significantly different from those found from the present data. We have searched all of the targets over again, starting from the ^{60}Ni result for the best large-angle polarization fit; but the $\chi_\sigma^2+\chi_P^2$ criterion leads back, by and large, toward the previous best-fit parameters (Table II).

It was pointed out by Lane[19] that the real part of the optical potential contains implicitly a term which depends on the isobaric spin. The isobaric spin, in turn, produces a dependence of the real potential on the

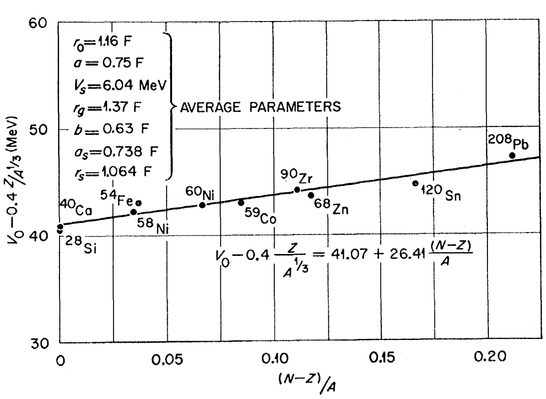

FIG. 8. Plot of the calculated real central potential minus its Coulomb dependence versus the symmetry parameter $(N-Z)/A$. The values of V_0 are from Table III and based on the average parameters shown in the figure. The straight line is a least-squares fit to the points. Here, $r_g=r_0'$ and $b=a'$.

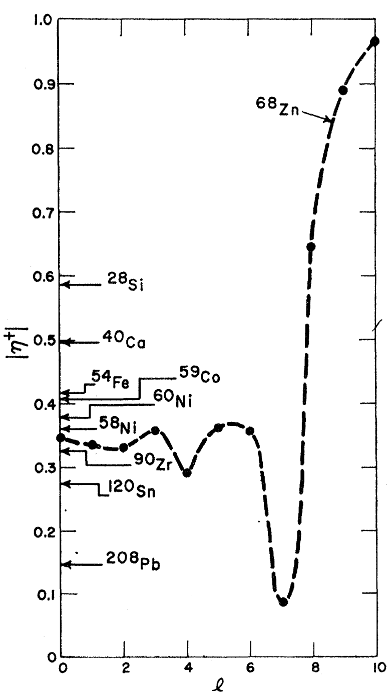

FIG. 9. Behavior of the absolute value of the reflection coefficient $|\eta^+|$ as a function of orbital angular momentum l for ^{68}Zn. The points are discrete values resulting from the optical-model fit to the 40-MeV proton elastic-scattering and polarization data. The dotted curve is just an aid to indicate the trend of the reflection coefficient with l. Arrows indicate the calculated values of $|\eta^+|$ at $l=0$ for the other 40-MeV data.

[17] L. N. Blumberg, R. H. Bassel, E. E. Gross, A. van der Woude, and A. Zucker, Bull. Am. Phys. Soc. 2, 103 (1965).

[18] D. A. Lind, D. E. Heagerty, and J. G. Kelly, Bull. Am. Phys. Soc. 2, 104 (1965); J. A. R. Griffith and S. Roman, Phys. Letters 19, 410 (1965); D. J. Baugh, J. A. R. Griffith, and S. Roman, Nucl. Phys. 83, 481 (1966); L. J. B. Goldfarb, G. W. Greenlees, and M. B. Hooper, Phys. Rev. 144, 829 (1966).

[19] A. M. Lane, Phys. Rev. Letters 8, 171 (1962).

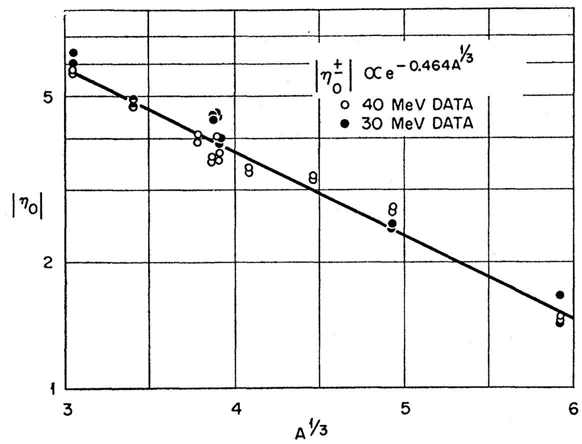

FIG. 10. Plot of the logarithm of the $l=0$ reflection coefficients as a function of $A^{1/3}$ for our 40-MeV data and existing 30-MeV data (Refs. 10, 11). The points result from optical-model fits to the data using the average parameters given in the text. The straight line appears to represent the trend of the data.

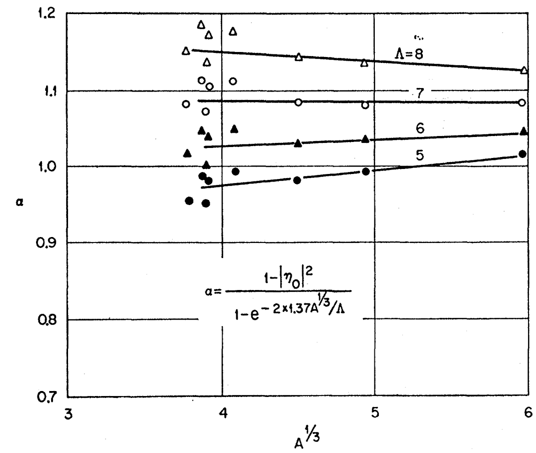

FIG. 11. Plot of α versus $A^{1/3}$ for various values of the mean free path for a reaction in nuclear matter, Λ. α is a ratio whose numerator is proportional to the probability that a beam proton suffers a reaction in an $l=0$ collision and whose denominator is the probability that a proton will not cross a nuclear diameter without suffering a reaction collision. Reflection coefficients for $l=0$ resulting from average-parameter fits were used to obtain the points.

nuclear-symmetry number $(N-Z)/A$. Perey[15] has analyzed a large amount of data between 9.5 and 22.2 MeV and found that indeed the real potential does show a dependence on the symmetry number. We have examined the variation of V_0 with $(N-Z)/A$ for our fixed-geometry optical-model parameters. We subtract from V_0 the A dependence which arises from the variation of the Coulomb potential with Z. Following Perey we take this correction to be $0.4\,Z/A^{1/3}$ MeV for $r_c=1.25$ F. In Fig. 8 we plot $V_0-0.4Z/A^{1/3}$ as a function of $(N-Z)/A$ for all our targets. The straight line which is obtained from a least-squares fit to the points is given by

$$V_0-0.4Z/A^{1/3}=41.1+26.4(N-Z)/A\,.$$

Thus the coefficient of the symmetry term in the optical potentisl is 26.4 MeV from our results. This is in excellent agreement with Perey,[15] who found a value of 27 MeV from an analysis of lower-energy data. Previous analyses of the 30-MeV data[10,11] give coefficients of 27,[14] 26,[12] and 20 MeV.[13]

As mentioned previously, our average parameters together with the potentials of Table IV also provide a fair fit to the 30-MeV data. Combining results from Tables III and IV, we infer an energy dependence of the real central well:

$$\frac{dV_0}{dE}=-0.22\pm0.03 \text{ (rms deviation)}.$$

This energy dependence is quite different than the value -0.3 found by Perey[15] from his analysis of lower-energy data, but some of this difference may be due to the use of different geometrical parameters. Recent cross-section measurements with 61.4-MeV protons have been analyzed[20] with the average parameters derived here, and the real central potentials obtained, together with those of Table III, are consistent with the dependence $dV_0/dE=-0.21$. For our average geometry then, a reasonable description of the real central well strength for protons in the energy range 30–40 MeV is provided by

$$V_0=49.9-0.22E+0.4Z/A^{1/3}+26.4(N-Z)/A\,,$$

where E is the proton energy in MeV.

It may be instructive to see what systematic information about nuclei can be extracted from the imaginary part of the optical-model potential. In particular we have investigated the behavior of the reflection coefficients η_l as a function of mass number. We find that $|\eta_l|$ plotted as a function of the orbital angular momentum l has a characteristic shape illustrated for ^{68}Zn in Fig. 9. For small values of l, $|\eta_l|$ is fairly flat with minor oscillations, it then dips sharply for a value of l close to the nuclear surface, and rises just as sharply to 1.0 for larger l values. Although only ^{68}Zn is illustrated, the other targets display very similar curves, except that the intercept at $l=0$ appears to be a nearly monotonic function of the atomic weight. Qualitatively, this is just what one would expect. As A increases, there is more nuclear matter, and in collisions where l is small, the probability of the proton coming out unscathed from the collision decreases. It appears possible then that the value of the $l=0$ intercept of $|\eta_l^{\pm}|$ may be related to the mean free path in nuclear matter, where the superscript on η_l refers to the proton spin being parallel (+) or antiparallel (−) to l. The

[20] C. B. Fulmer, J. B. Ball, A. Scott, and M. L. Whiten (to be published).

$l=0$ intercept was calculated separately for $|\eta^+|$ and $|\eta^-|$ by averaging the reflection coefficients for the first few l values; we define $|\eta_0^\pm|$ as being that average. This method averages over the minor oscillations at small l and should give a better value for the $l=0$ intercept.

First we note that $|\eta_0^\pm|$ is an exponential function of the nuclear radius. In Fig. 10 the same straight line,

$$|\eta_0| \propto \exp[-0.464A^{1/3}],$$

fits both the 30- and 40-MeV results.

A correlation between $|\eta_0|$ and the mean free path for a reaction in nuclear matter Λ can be established as follows. The reaction cross section σ_{R_0} for $l=0$ protons is given by

$$\sigma_{R_0}/\pi\lambda\!\!\!^{-2}=1-|\eta_0|^2.$$

For $l=0$ protons, the path length through nuclear matter in a nucleus of mass number A is expected to be nearly $2r_0'A^{1/3}$, and the probability for a reaction should be $[1-\exp(-2r_0'A^{1/3}/\Lambda)]$. Therefore we have

$$1-|\eta_0|^2=\alpha[1-\exp(-2r_0'A^{1/3}/\Lambda)],$$

where α should be a constant for all nuclei whose diameters are large compared to Λ. In Fig. 11 we plot α versus $A^{1/3}$ for various values of Λ for mass numbers greater than 40. A value of $\Lambda=7$ F appears to produce the proper dependence of α as a function of $A^{1/3}$.

A WKB calculation by Drisko[21] treating our Pb data with a "strong-absorption" model leads to $\Lambda=6.0$ F and $\alpha=1.0$, whereas the value of α inferred from Fig. 11 is about 1.1.

ACKNOWLEDGMENTS

The authors wish to thank R. H. Bassel, R. M. Drisko, and G. R. Satchler for valuable discussions regarding the optical-model calculations and interpretation of the results. Our thanks also to L. N. Blumberg who participated in the early phases of this work, and to R. W. Rutkowski who helped with some of the calculations. We are indebted to the operating crews of ORIC for their superlative efforts in maintaining steady proton beams over long periods. We acknowledge with pleasure the support of R. S. Livingston and A. H. Snell in all phases of this work.

[21] R. M. Drisko (private communication).